frontiers in
NEURAL CIRCUITS

ORIGINAL RESEARCH ARTICLE
published: 22 November 2011
doi: 10.3389/fncir.2011.00017

Endocannabinoid release modulates electrical coupling between CCK cells connected via chemical and electrical synapses in CA1

Jonathan Iball and Afia B. Ali*

Department of Pharmacology, The School of Pharmacy, University of London, London, UK

Edited by:
Miles A. Whittington, Newcastle University, UK

Reviewed by:
Brian Antonsen, Marshall University, USA
Mark Cunningham, University of Newcastle, UK

****Correspondence:***
Afia B. Ali, Department of Pharmacology, The School of Pharmacy, University of London, 29/39 Brunswick Square, London WC1N 1AX, UK.
e-mail: afia.ali@pharmacy.ac.uk

Electrical coupling between some subclasses of interneurons is thought to promote coordinated firing that generates rhythmic synchronous activity in cortical regions. Synaptic activity of cholecystokinin (CCK) interneurons which co-express cannabinoid type-1 (CB1) receptors are powerful modulators of network activity via the actions of endocannabinoids. We investigated the modulatory actions of endocannabinoids between chemically and electrically connected synapses of CCK cells using paired whole-cell recordings combined with biocytin and double immunofluorescence labeling in acute slices of rat hippocampus at P18–20 days. CA1 stratum radiatum CCK Schaffer collateral-associated cells were coupled electrically with each other as well as CCK basket cells and CCK cells with axonal projections expanding to dentate gyrus. Approximately 50% of electrically coupled cells received facilitating, asynchronously released inhibitory postsynaptic potential (IPSPs) that curtailed the steady-state coupling coefficient by 57%. Tonic CB1 receptor activity which reduces inhibition enhanced electrical coupling between cells that were connected via chemical and electrical synapses. Blocking CB1 receptors with antagonist, AM-251 (5 μM) resulted in the synchronized release of larger IPSPs and this enhanced inhibition further reduced the steady-state coupling coefficient by 85%. Depolarization induced suppression of inhibition (DSI), maintained the asynchronicity of IPSP latency, but reduced IPSP amplitudes by 95% and enhanced the steady-state coupling coefficient by 104% and IPSP duration by 200%. However, DSI did not did not enhance electrical coupling at purely electrical synapses. These data suggest that different morphological subclasses of CCK interneurons are interconnected via gap junctions. The synergy between the chemical and electrical coupling between CCK cells probably plays a role in activity-dependent endocannabinoid modulation of rhythmic synchronization.

Keywords: CA1, CB1, CCK, DSI, electrically coupled, endocannabinoids, interneurons

INTRODUCTION

Network oscillations are thought to be generated by combined synchronous entrainment of inhibitory postsynaptic potentials (IPSP) onto pyramidal cells. Moreover interneurons that are interconnected electrically promote coordinated firing, contributing to the generation, and stability of rhythmic synchronous network activity in several brain regions (Galarreta and Hestrin, 1999; Gibson et al., 1999; Koos and Tepper, 1999; Hormuzdi et al., 2001; Best and Regehr, 2009). In the central nervous system electrical coupling has been reported to exist due to gap junctions between dendrites (Sloper, 1972; Kosaka and Hama, 1985) as well as axons and soma and dendrites (Pappas and Bennett, 1966; Tamas et al., 2000).

The diverse sub-populations of interneurons are characterized by criteria such as neurochemical marker expression, dendritic and axonal morphology, and electrophysiological properties (Freund and Buzsaki, 1996; Somogyi and Klausberger, 2005). Often electrical synapses are made specifically among interneurons belonging to the same subclass and one such subtype being the parvalbumin expressing fast spiking interneuron, thought to be responsible for gamma frequency oscillation (Cobb et al., 1995; Gibson et al., 1999; Tamas et al., 2000; Blatow et al., 2003; Mancilla et al., 2007; Hjorth et al., 2009). However, recent studies have demonstrated that several other non-fast spiking subclasses of interneurons in the neocortex are interconnected via electrical synapses, including neocortical irregular-spiking interneurons that express cannabinoid type-1 (CB1) receptors (Galarreta et al., 2004, 2008 see also, Gibson et al., 1999) and calretinin interneurons (Caputi et al., 2009). The exception to this rule seems to be the neuroglia form (NGF) cell, as they are coupled electrically with each other as well as to other interneuron subclasses in the neocortex (Simon et al., 2005). Whether parallels exist in the hippocampal network of non-fast spiking interneurons needs to be investigated.

A specific group of hippocampal CA1 interneurons expressing cholecystokinin (CCK) often co-express CB1 receptors (Katona

Abbreviations: AM-251, 1-(2,4-dichlorophenyl)-5-(4-iodophenyl)-4-methyl-*N*-(1-piperidyl)pyrazole-3-carboxamid; CB1, cannabinoid receptor type-1; CCK, cholecystokinin; DSI, depolarization induced suppression of inhibition; IPSP, inhibitory postsynaptic potential; LM–PP, lacunosum moleculare–perforant path; SCA, Shaffer collateral-associated; VIP, vasoactive intestinal polypeptide.

et al., 1999; Marsicano and Lutz, 1999; Bodor et al., 2005). CB1 receptors are involved in a variety of activity including mediating depolarization induced suppression of inhibition (DSI; Llano et al., 1991; Ohno-Shosaku et al., 2001; Wilson and Nicoll, 2001; Ali, 2007) and in modulating rhythmic oscillatory activity by disrupting spike timing (Hajós et al., 2000; Robbe et al., 2006). Previously it has been demonstrated that these cells in CA1 can make dual electrical and chemical synapses with each other (Ali, 2007), however the role for this dual connectivity between CCK cells has not been investigated and there is still much to be understood about the specific roles of CCK hippocampal interneurons. CCK cells that are connected chemically have the ability to allow more temporal and spatial flexibility as they can switch between synchronous and asynchronous release of GABA via CB1 receptors (Ali and Todorova, 2010). Whether these modulatory actions extend to modulating electrically coupled CCK synapses that are also paired with chemical synapses was investigated using dual whole-cell recordings combined with biocytin and double immunofluorescence labeling in acute slices of P18–20 day old rat hippocampus.

EXPERIMENTAL PROCEDURES

SLICE PREPARATION

Male Wistar rats (postnatal day, P18–20) were anesthetized by an intraperitoneal injection of sodium Pentobarbitone (60 mg kg^{-1} Euthatal, Merial, UK) and perfused transcardially with 50–100 ml ice-cold modified artificial cerebrospinal fluid (ACSF). This modified ACSF contained (mM): 248 sucrose, 25.5 $NaHCO_3$, 3.3 KCl, 1.2 KH_2PO_4, 1.0 $MgSO_4$, 2.5 $CaCl_2$, and 15 D-glucose, equilibrated with 95% O_2/5% CO_2. The animals were then decapitated and the brain removed, these procedures were reviewed by ethical committees and comply with British Home office regulations for the use of animals.

Coronal sections of cerebral cortex and hippocampus, 300 μm thick, were cut using a vibratome (Leica, Germany). The slices were incubated for 1 h in standard ACSF containing (in mM): 121 NaCl, 2.5 KCl, 1.25 NaH_2PO_4, 2 $CaCl_2$, 1 $MgCl_2$, 26 $NaHCO_3$, 20 glucose and 5 pyruvate, and equilibrated with 95% O_2/5% CO_2. For recordings, slices were transferred to a submerged-style chamber and perfused at 1–2 ml/min with the standard ACSF.

PAIRED RECORDINGS

Simultaneous dual whole-cell somatic recordings were made in current clamp between electrophysiologically identified CA1 stratum radiatum (SR) and stratum lacunosum moleculare (SLM) interneurons. Cells of each recorded pair were visually selected using video-microscopy under near-infrared differential interference contrast (DIC) illumination. Interneurons were selected with round or oval somata and further characterized from their firing properties. Experiments were conducted at room temperature (20–22°C) with patch pipettes (resistance 8–10 MΩ) pulled from borosilicate glass tubing and filled with an internal solution containing (in mM): 144 K-gluconate, 3 $MgCl_2$, 0.2 EGTA, 10 HEPES, 2 Na_2-ATP, 0.2 Na_2-GTP, and 0.02% w/v of biocytin (pH 7.2–7.4, 300 mOsm).

Trains of presynaptic action potentials were elicited by injecting 200 ms pulses of 0.1 nA, depolarizing current into the presynaptic interneuron, repeated at 0.33 Hz (SEC 05L/H, npi electronics, GmbH, Germany). Postsynaptic interneurons were held at between −55 and −70 mV. Electrical synapses between pairs of interneurons were studied by injecting 200 ms current pulses ranging from −0.05 to +0.1 nA in one cell and observing the passive transfer in the other (postsynaptic cell) at several different membrane potentials.

Postsynaptic responses recorded in interneurons were amplified, low-pass filtered at 2 kHz, digitized at 5 kHz using a CED 1401 interface, and recorded on disk for off-line analysis.

DSI protocol

Depolarization induced suppression of inhibition was induced by depolarizing the postsynaptic membrane by injecting a 200-ms depolarizing step that elicited a train of three to five action potentials, followed by the depolarizing or hyperpolarizing steps of 200 ms in the presynaptic cell. These steps were elicited 900 ms after the end of the postsynaptic depolarizing step to allow the complete relaxation of the postsynaptic membrane currents. The postsynaptic membrane potential was held at −55 mV, for periods of 1.5 s repeated at 0.33 Hz. In control conditions (pre DSI) the presynaptic action potentials or hyperpolarizing steps were elicited without any postsynaptic depolarization. The duration of recording during pre and post DSI protocols was 90 s, which included 30 frames of synaptic/electrical events collected. Averages of IPSPs or voltage transfer were made from steady-state responses during DSI, reached within 20–30 s.

Drugs

Pharmacology was performed on pairs of cells that were connected chemically and electrically coupled.

Data were collected in the presence of bath applied, CNQX and D-AP5 (50 μM), MCPG (1 mM), CPPG (100 μM), and CPG55845 (100 μM), naloxone (100 μM) to block AMPA/kainate, NMDA, mGluR, $GABA_B$, and opioid receptors, respectively (all from Tocris Bioscience, UK). CB1 receptor antagonists, AM-251 (5 μM; Tocris, UK) was used to study the CB1 receptor pharmacology of IPSPs elicited by Schaffer collateral-associated (SCA) interneurons.

Data analysis

Data were acquired and analyzed using Signal software (Cambridge Electronic Design, Cambridge, UK). The electrophysiological characteristics of the recorded cells were measured from their voltage responses to 500 ms current pulses between −0.2 and +0.1 nA in amplitude. Averaging of IPSPs was triggered from the rising phase of the presynaptic spike. Amplitudes of a postsynaptic event were defined as the difference between the peak amplitude and the baseline value before the onset of the IPSP. The IPSP 10–90% rise times, peak amplitude, and width at half amplitude were measured from averaged IPSPs. IPSP latencies were manually measured as the time delay between presynaptic action potential peaks to the onset of the detectable IPSPs. The fluctuations in the IPSP latencies were quantified in non-overlapping time interval sets of 5 ms after each presynaptic action potential. To obtain estimations of synchronous to asynchronous release the frequency of IPSPs at set-time intervals were measured manually. Synchronous release was taken as release of neurotransmitter (unitary voltage

change in the postsynaptic cell, filtered at 2 kHz) within 0–5 ms latencies, whereas asynchronous release was taken as the change in voltage falling within a time window of 5–15 ms latencies. The synchronicity ratio was calculated from the estimated ratio of synchronous release/asynchronous release (from data set of 100–300 sweeps).

Coupling coefficients were calculated as the ratio between the change of voltage transfer in the non-injected cell and that of the current injected cell. Steady-state coupling coefficients are referred to averaged transfer of hyperpolarizing and depolarizing pulses without resulting in action potentials. Electrical transfers which were mixed with IPSPs elicited in postsynaptic cells were measured from the baseline to the maximum point of transfer within 3–10 ms before the onset of IPSPs. Depolarizing pulses resulting in presynaptic action potentials which were transferred passively to the postsynaptic cell are referred to as "spikelets." These spikelets were measured from the onset to the peak of the depolarizing phase of the passive transfer in the postsynaptic cell. Spike coupling coefficients refer to spikelets.

Data are given as mean ± SD obtained from 50 to 250 sweeps, graph plots illustrate averaged data from individual paired recording data and average population data ± SE. Statistical significance was analyzed by Student's paired or unpaired *t*-test.

MORPHOLOGY

Slices containing biocytin-filled cells were fixed overnight in 4% Para formaldehyde plus 0.2% saturated picric acid solution in 0.1 M phosphate buffer (PB), pH 7.4 at 4˚C for immunofluorescence or in 1.25% glutaraldehyde and 2.5% paraformaldehyde in 0.1 M PB for standard Avidin–HRP–DAB processing (see below). Extensive rinses were carried out between each step using phosphate buffered saline (PBS 0.1 M). The sections were freeze–thawed over liquid nitrogen after cryoprotecting for 2 × 10 min in 10% sucrose, 2 × 20 min in 20% sucrose with 6% glycerol, and 2 × 30 min in 30% sucrose and 12% glycerol. The sections then followed either a double immunofluorescence (shorter recordings of 10–40 min) or a standard biocytin labeling protocol for longer recording (40–90 min).

DOUBLE IMMUNOFLUORESCENCE

After rapid freeze–thawing, the sections were washed in PB, and then incubated in 1% sodium borohydride ($NaBH_4$) solution in 0.1 PB for 30 min. After further washes in PB to remove $NaBH_4$ slices were incubated in normal blocking serum diluted in 0.1 M phosphate buffer saline (PBS) for 30 min. Both fluorescent-tagged secondary antibodies used were raised in goat, 10% normal goat serum (Sigma). The cells recorded in this study were incubated in antibodies to vasoactive intestinal peptide (VIP) and CCK. The rationale for using both these antibodies is that SR and lacunosum moleculare cells are usually CCK or VIP positive. These antibodies were raised against different antigenic targets, e.g., rabbit anti-VIP (B 34-1, source, Euro-Diagnostica B V, NETH, 1:1000 dilutions) and mouse anti-gastrin/CCK (gift, source, Cure antibody laboratory, UCLA, 1:2000 dilution). Primary antibody mixtures were made up with 3 mg bovin serum albumin (BSA; Sigma) per ml of diluents containing peroxidase-labeled ABC Elite (ABC-peroxidase; Vector Laboratories) made in PBS and incubated over night. The sections were washed in PBS prior to incubating in secondary antibodies and avidin macromolecules tagged with different fluorescent markers. This cocktail contained goat anti-rabbit IgG (diluted to 1:600, Molecular Probes) conjugated to Texas red, goat anti-mouse IgG (diluted 1:160; Sigma) conjugated to FITC and Avidin conjugated to AMCA (1:250, Vector laboratories). Following 3 h of incubation at room temperature, the sections were washed in PBS and mounted onto glass slides in 50% glycerol in PBS and cover slipped. The sections were then examined for fluorescent labeling using a Leica DMR microscope with appropriate filter blocks to visualize FITC, Texas red, and AMCA respectively at ×40 magnification. Following immunohistochemical detections the sections were processed to reveal the biocytin labeled cells as described below.

BIOCYTIN LABELING

The sections were incubated overnight in Vector ABC-peroxidase (1:200) at 4˚C. The peroxidase group was revealed using 3′3 diaminobenzidine as the chromogen (Vector DAB kit). The visualized cells were intensified with 1% osmium tetroxide and the sections were cleared by dehydration in an ascending series of alcohols to 100%, and then embedded in Durcupan resin (Agar Scientific). The cells were reconstructed using a Zeiss Axioskop with attached camera lucida. Morphometric analysis was performed manually from two dimensional reconstructions of neurons.

The classification of interneurons was based on electrophysiology, neurochemistry, and on gross morphology (Freund and Buzsaki, 1996; Somogyi and Klausberger, 2005).

RESULTS

To determine the extent of electrical coupling in CA1 SR/SLM, dual whole-cell recordings between interneurons were made. From 38 experiments and 270 pairs of interneurons tested for electrical connections, 23 interneuronal pairs were electrical coupled, of which 9 electrically coupled pairs were also innervated chemically, 4 of which were reciprocal chemical connections.

MORPHOLOGICAL AND MEMBRANE PROPERTIES OF CCK INTERNEURONS

Cholecystokinin-positive SCA cell bodies were found in SR and SLM. Their dendritic fields expanded to all layers in CA1 and were smoothly beaded in appearance. Their axons ramified predominantly in SR with some branches passing stratum pyramidale (SP) and extended into stratum oriens (SO; $n = 31$). **Figure 1** illustrates the morphological properties of two connected CCK-positive SCA interneurons. Approximately, 55% of pairs tested for electrical coupling were revealed as two SCA cells.

Cholecystokinin-positive lacunosum moleculare–perforant path (LM–PP) interneuron cell bodies were located in the border of SR/SLM, their sparsely spiny dendrites extended horizontally along the border of SR and SLM, with vertical branches entering SLM. Their axonal arborization ramified in stratum lacunosum molecular and extended to the dentate gyrus ($n = 7$). **Figure 2** illustrates an example of the morphological properties of LM–PP associated interneurons. On average a single LM–PP cell was tested with three other interneurons before finding an electrical connection.

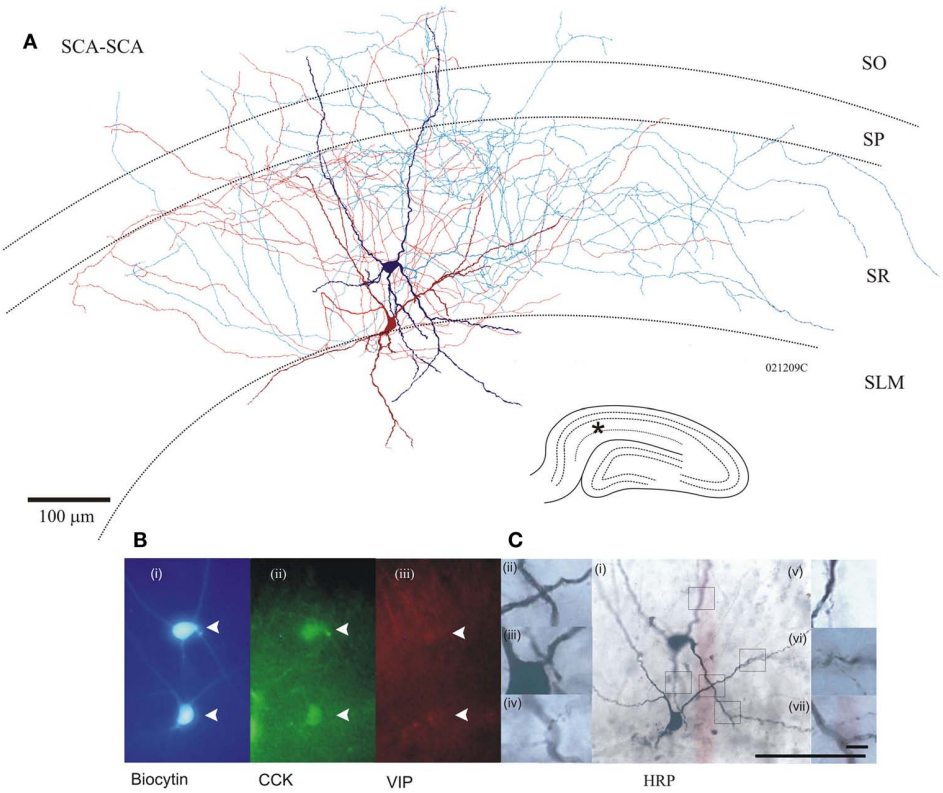

FIGURE 1 | (A) Anatomy of two Schaffer collateral-associated (SCA) cholecystokinin (CCK) positive cells reciprocally, chemically connected and electrically coupled (see **Figure 4** for electrophysiological properties), dark red/blue cell soma, and dendrites corresponds with light red/blue axon, respectively. Inset bottom right, hippocampal schematic with asterisk marking location of paired recordings. **(B)** Photomicrographs of fluorescence labeling using epifluorescent microscope (i) in blue, AMCA-Avidin labeling of biocytin-filled pair, (ii) green shows positive CCK labeling of biocytin-filled cells (closed arrows); (iii) in red, VIP labeling showing absence of staining in cells of interest. **(C)** Permanent DAB staining of above cells, with boxes representing location of magnified pictures (i). Close apposition between proximal dendrites of two cells (ii, iii). Putative autapse of dark blue cell (iv, v). Putative synaptic connection, blue to red (vi), and red to blue (vii). Bottom scale bar, 100 μm [for (i) and Fluorescent images], top Scale bar 10 μm (for ii–vii).

Cholecystokinin-positive SP basket cell body was located in SP, with dendrites radiating vertically into SO and SR, fine dendritic branches terminated into SLM. The axons of these cells densely innervated SP (see Ali et al., 1999; $n = 4$). On average a single SP basket cell tested with 6 other interneurons before finding an electrical connection was found between them.

The intrinsic membrane properties of SCA and LM–PP cells were similar and displayed fast adapting firing patterns. The action potential widths were, 1.7 ± 0.42 and 1.4 ± 0.42 ms for SCA and LM–PP cells, respectively. The action potentials terminated with a shallow after-hyperpolarizations and trains of spikes showed accommodation or spike frequency adaptation (see **Figures 2C,D** for examples of firing properties). The input resistances and the membrane time constants were, 297 ± 46 and 342 ± 74 MΩ and 24 ± 4.3 and 29 ± 4.5 ms for SCA ($n = 12$) and LM–PP ($n = 7$) interneurons, respectively.

Basket cells displayed similar adapting firing properties, average action potential widths were 1.5 ± 0.6 ms with average input resistance and membrane time constant of, 320 ± 90 MΩ and 25 ± 5 ms, respectively ($n = 4$).

COMMUNICATION SOLELY VIA ELECTRICAL COUPLING BETWEEN CCKs

Schaffer collateral-associated–SCA cell pairs that were closely spaced (5–10 μm between somata) were electrical coupled and putative somato-dendritic and dendro-dendritic contacts were revealed by light microscopic analysis (SCA–SCA, $n = 6$). The average electrical distance from soma to putative contact was, 42 ± 13.5 μm ($n = 6$). However, interneuronal pairs that were some distance apart (10–50 μm from somata to contact) were also found to be electrically coupled, these included SCA–LM–PP cells ($n = 4$) and SCA–BC ($n = 4$) connections. Putative somato-dendritic and dendro-dendritic close contacts (average distance from soma, 101 ± 5 μm) were seen between SCA–LM–PP cells, whereas close contacts between dendrites (average distance from soma, 110 ± 15 μm) were only observed between SCA–BC pairs revealed by light microscopic analysis.

Electrical coupling were determined by injection of depolarizing and hyperpolarizing current pulses that produced direct passive voltage changes in the non-current injected cell. **Figures 3A,B** illustrate examples of electrical coupling between SCA–SCA and SCA–BC connections.

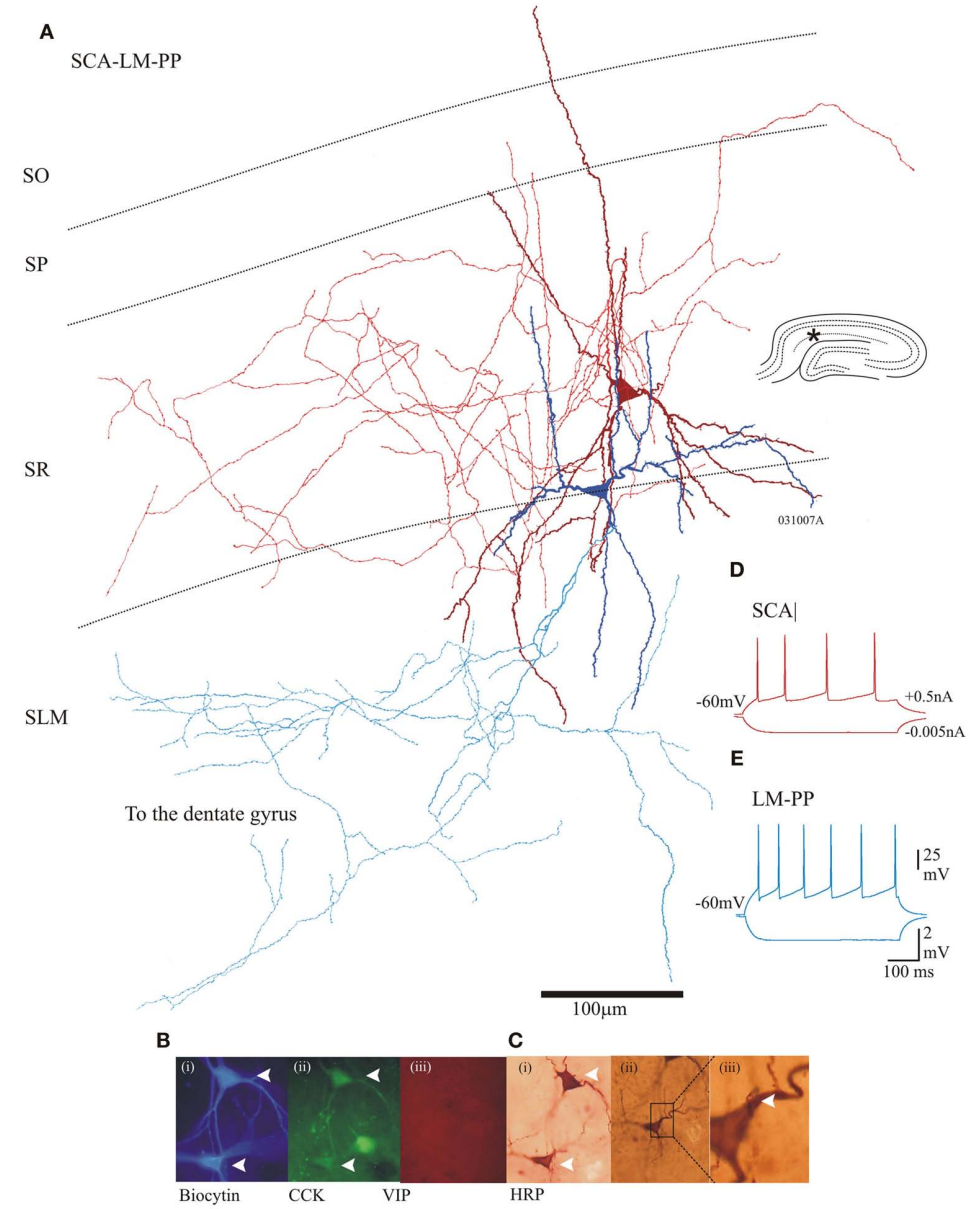

FIGURE 2 | Properties of two morphologically different CCK cells that were electrically coupled. (A) Reconstruction of SCA (dark red dendrites and red axon) and a lacunosum moleculare–perforant path associated cell (LM–PP, dark Blue dendrites and light blue axon). Insert (right) is a hippocampal schematic with an asterisk marking the location of the recordings. **(B)** Immunofluorescence labeling using epifluorescent microscope: (i) in blue, AMCA-Avidin labeling of biocytin-filled pair, (ii) green shows positive CCK labeling of biocytin-filled cells (closed arrows); (iii) in red, VIP labeling showing absence of staining in cells of interest. **(C)** (i) Photomicrograph of a permanent DAB-stain of both cells. (ii) An SCA to LM–PP dendro-somatic apposition, which is shown enlarged in (iii). **(D,E)** Adapting firing properties of the recorded SCA and LM–PP cells in response to −0.005 and +0.5 nA current injection.

Electrical transmission at connections solely connected via electrical synapses was bidirectional and symmetrical at SCA–SCA connections (bidirectional transfer was not significantly different, $p \geq 0.8$, $n = 6$, **Figure 3A** right panel). However, there was a asymmetric difference in the magnitude of the transfer which was stronger in one direction for steady-state coupling between heterogeneous subclasses of interneurons; SCA–LM–PP cells and SCA–BC connections (paired t-test, $p \leq 0.05$, $n = 8$, **Figure 3B**, right panel) and between interneurons that were connected via both, chemical and electrical synapses (see next section). This asymmetrical steady-state coupling was similar to previous observations where data for both types of connections were pooled (Ali, 2007).

Steady-state electrical coupling potentials were in the range of 0.01 and 3.2 mV in amplitudes with transfer duration in the range of 147 and 250 ms measured at half amplitude (in response to 200 ms current pulse) at -64 ± 2 mV. Electrical coupling followed presynaptic action potentials with a delay of 3 and 18 ms measured from the rising phase of the presynaptic action potential

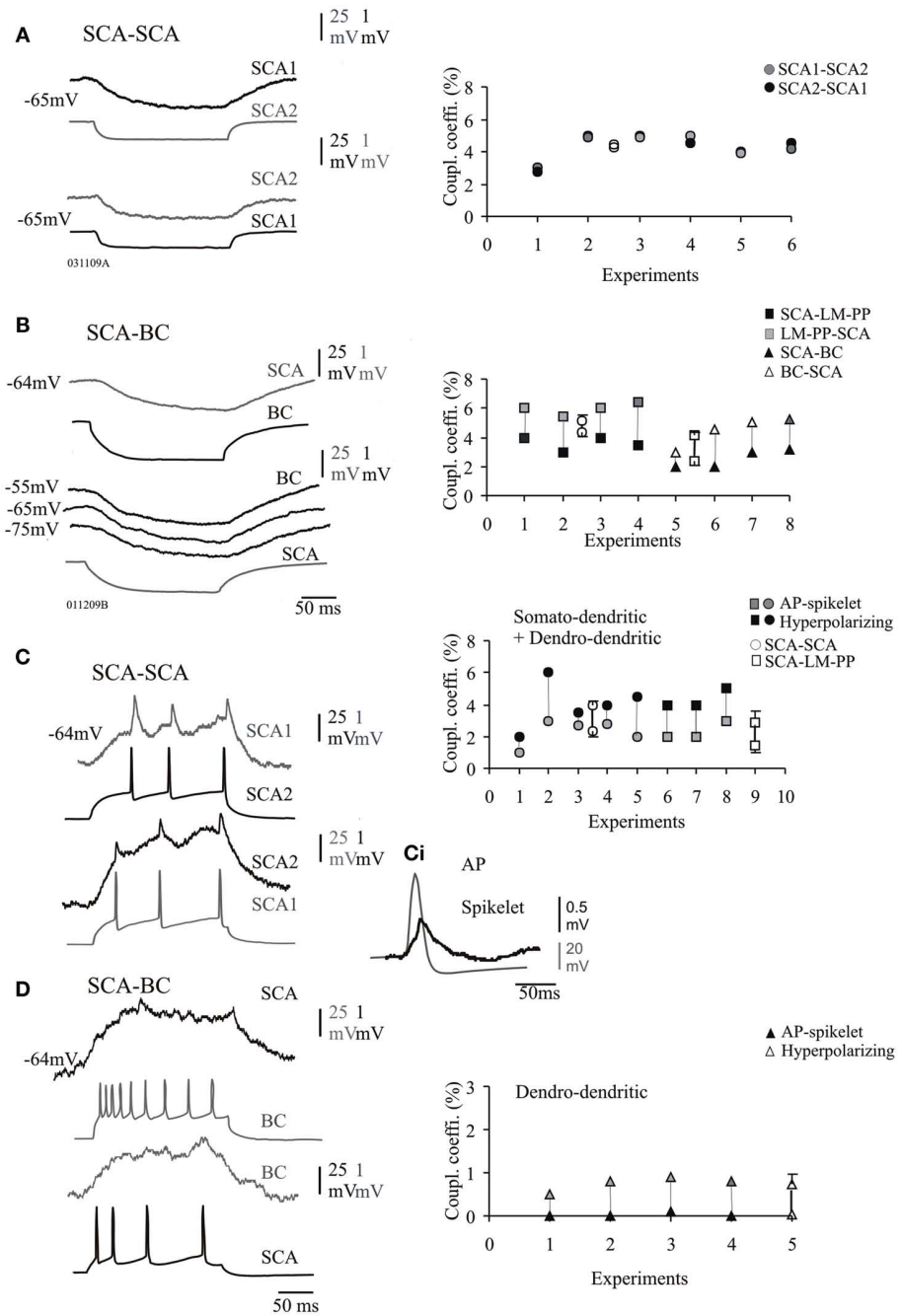

FIGURE 3 | Electrical synapses between CCK cells. (A) Pair of SCA cells connected electrically, the average passive transfer of voltage was always reciprocal and transfer in both directions recorded at −65 mV is shown. Right panel shows the steady-state coupling coefficient at individual SCA–SCA cell pairs, which were symmetrical if coupled solely via electrical synapses (average values are represented by empty symbols). **(B)** Pair of SCA and a basket cell (BC) electrically coupled. The passive transfer of voltage was asymmetric at connections between morphologically different CCK cells (BC and LM–PP cells). The steady-state coupling coefficient was lower in the direction from SCA cells correlated with the lower input resistance of SCA compared to LM–PP and BC cells. **(C)** Action potentials (APs) in SCA cell 1 is reflected as spikelets in SCA cell 2. **(Ci)** A presynaptic action potential and a spikelet are superimposed and shown on a larger scale. The adjacent plots illustrate the spike coupling coefficients from individual pairs of SCA–SCA and SCA–LM–PP cell connections which were seen to have close somato-dendritically and dendro-dendritic contacts at the light microscope level. **(D)** The spike coupling coefficient was not efficient at electrical connections between SCA and BC, interestingly close dendro-dendritic contacts were observed only at the light microscope level for these connections. There was a general trend in the efficiency of transmission, spike coupling coefficient (due to fast APs) was lower compared to the transfer of the longer hyperpolarizing phase of the APs, shown for both, somato-dendritic and dendro-dendritic groups shown in the right panels of **(C,D)**, average values ± SE are represented by empty symbols (*x*-axis represents individual pairs).

to the onset of the passive membrane change of the steady-state electrical coupling.

Figure 3 illustrates the steady-state coupling coefficient for all the pairs that were coupled electrically only, there was a significant difference in the steady-state coupling coefficient between SCA–SCA cells and SCA-heterogeneous subclasses (unpaired *t*-test, $p \leq 0.05$, $n = 7$). The average coupling coefficients among SCA–SCA cell pairs was $4.2 \pm 0.8\%$ in one direction and $4.3 \pm 0.8\%$ in the opposite direction ($n = 6$). The average steady-state electrical coupling between SCA–LM–PP and SCA–BC was, $4.3 \pm 1.2\%$ ($n = 4$) and $2.5 \pm 0.5\%$ ($n = 4$) in one direction (from SCA cells) and 5.2 ± 0.9 and $4.4 \pm 0.9\%$ in the opposite direction (from LM–PP and BCs) at -60 mV, respectively. This asymmetric coupling coefficient was positively correlated with differences in the input resistances; the higher input resistance of LM–PP cells and BCs, was related to the greater steady-state coupling coefficients ($r = 0.92$, $p < 0.05$, $n = 8$). Under different membrane potentials the passive transfer of voltage was similar in BCs (and LM–PP cells, data not shown), shown in **Figure 3B**, suggesting these cells did not rectify and that rectification of voltage was not the cause of the asymmetrical differences observed.

Similar asymmetric differences were seen between multipolar and bipolar calretinin cells in the neocortex due to their differences in the input resistances (Caputi et al., 2009).

To study the filter properties of the symmetrical and asymmetrical electrical coupling, the coupling coefficient for transmission of hyperpolarizing and depolarizing currents were compared. At SCA–SCA and SCA–LM–PP connections the action potentials transferred through electrically coupled CCK cells, during supra-threshold depolarizing current pulses that elicited short-lasting action potentials resulted in corresponding spikelets in the postsynaptic cells that were biphasic consisting of depolarizing and hyperpolarizing components (see **Figure 3C**). The depolarizing action potential transfer into spikelets were in the range of 0.01 and 0.03 mV and the average spike coupling coefficient was $2.3 \pm 0.8\%$ for SCA–SCA connections and $1.4 \pm 1.3\%$ for SCA–LM–PP connections at -64 ± 2 mV. The spike coupling coefficients were membrane potential dependent and at a more negative membrane potential of -72 ± 3 mV, there was a reduced transfer of, $0.6 \pm 1\%$ for SCA–SCA connections and $0.4 \pm 0.5\%$ for SCA–LM–PP connections. At SCA–BC connections the average spike coupling coefficient was $0.03 \pm 0.35\%$. The hyperpolarizing component reflecting spike after-hyperpolarizations was in the range of 0.02 and 0.1 mV (average, $4.1 \pm 0.5\%$ for SCA–SCA connections ($n = 6$) and $2.8 \pm 2.0\%$ for SCA–LM–PP connections) and in the range of 0.005 and 0.011 mV (average, $0.7 \pm 0.3\%$, $n = 4$) for SCA–BC cell connections. Note that the filtering properties were more pronounced at SCA–BC cell connections, as single or trains of actions potentials in one cell resulted in weaker passive transfer of action potentials and after-hyperpolarizations in the non-current injected cells.

DUAL CONNECTIVITY VIA CHEMICAL AND ELECTRICAL COUPLING OF CCK CELLS

Dual connectivity via $GABA_A$ receptor mediated chemical synapses and electrical coupling will be the focus here. These synapses were always seen to have close somato-dendritic, as well as dendro-dendritic close contacts observed at the light microscope level ($n = 9$). **Figure 4B** illustrates the steady-state coupling coefficient in response to 200 ms hyperpolarizing current injection for individual pairs that were coupled electrically and chemically, steady-state coupling coefficient was asymmetric (see **Figure 4A**). The average steady-state coupling coefficients at -70 mV was $3 \pm 1.2\%$ in one direction and $4.1 \pm 1.5\%$ in the opposite direction for SCA–SCA connections ($n = 5$) and $5 \pm 1.6\%$ in one direction and $8 \pm 1.4\%$ in the opposite direction for SCA–LM–PP connections ($n = 3$). **Figure 4E** illustrates the difference in spike coupling coefficients of these synapses connected electrically and chemically, average spike coupling coefficients were, 0.3 ± 0.2 and $0.4 \pm 0.08\%$ for SCA–SCA and SCA–LM–PP connections, respectively. The average transfer of the after-hyperpolariztion phase of spikes were, 3.5 ± 1 and $8 \pm 1.4\%$ for SCA–SCA ($n = 5$) and SCA–LM–PP ($n = 3$) connections, respectively.

Presynaptic firing (at 25–40 Hz) elicited IPSPs which displayed brief train facilitation (see **Figures 4C,D**). Unitary chemical synapses between SCA and SCA have been reported previously (see Ali, 2007, 2011; Ali and Todorova, 2010; for details of short-term plasticity). The postsynaptic responses were composed of electrical spike coupling potentials followed by IPSPs elicited after long-latencies (range, 3 and 7 ms, average, 4.3 ± 3.5 ms). The first IPSPs usually averaged between 0 and 0.05 mV, due to a high proportion of synaptic failures. The average amplitude of second IPSPs were, 1.09 ± 0.6 mV. The average first IPSP rise time and width at half amplitude was, 7 ± 0.9 and 45 ± 8 ms, respectively ($n = 9$).

TONIC ACTIVATION OF CB1 RECEPTORS ENHANCES ELECTRICAL COUPLING

The amplitudes and the duration of electrical coupling potentials were reduce during repetitive presynaptic firing that elicited trains of IPSPs in control conditions at synapses connected via electrical and chemical innervations. The coupling coefficient during presynaptic firing of 25 Hz was, $0.5 \pm 0.16\%$ with a duration of 14 ± 3 ms (pooled data for SCA–SCA and SCA–LM–PP connections, $n = 9$), compared to the steady-state coupling coefficient of $1.2 \pm 0.3\%$ during presynaptic firing resulting in no IPSPs at a membrane potential close to chloride ion reversal potential of -70 ± 2 mV (**Figures 4C,D**, $p = 0.05$, $n = 9$). This suggests that the IPSPs curtailed the passive transfer of voltage. CB1 receptor antagonist, AM-251, increased IPSP peak amplitudes suggesting a tonic suppression of inhibition via CB1 receptors (see Ali and Todorova, 2010). During bath application of AM-251, the average first IPSP amplitudes increased to, 2.5 ± 1.08 mV (120% larger than control, $p \leq 0.05$, $n = 8$), this increased inhibition curtailed the spike coupling coefficient further to, $0.08 \pm 0.11\%$ (see **Figure 4F** for individual connections). The enhanced inhibition was also accompanied by reduced asynchronous release and increased synchronicity ratio of, 5.6 ± 1.2 (control, synchronicity ratio was, 0.6 ± 0.53, $p \leq 0.05$, $n = 8$, see also, Ali and Todorova, 2010). The increased synchronicity was accompanied by a reduced average IPSP latency of, 3.5 ± 0.95 ms (average control latency, 4.3 ± 3.5 ms). This is also reflected in the shorter duration of the first spikelet transfer of, 7.5 ± 2.3 ms during AM-251.

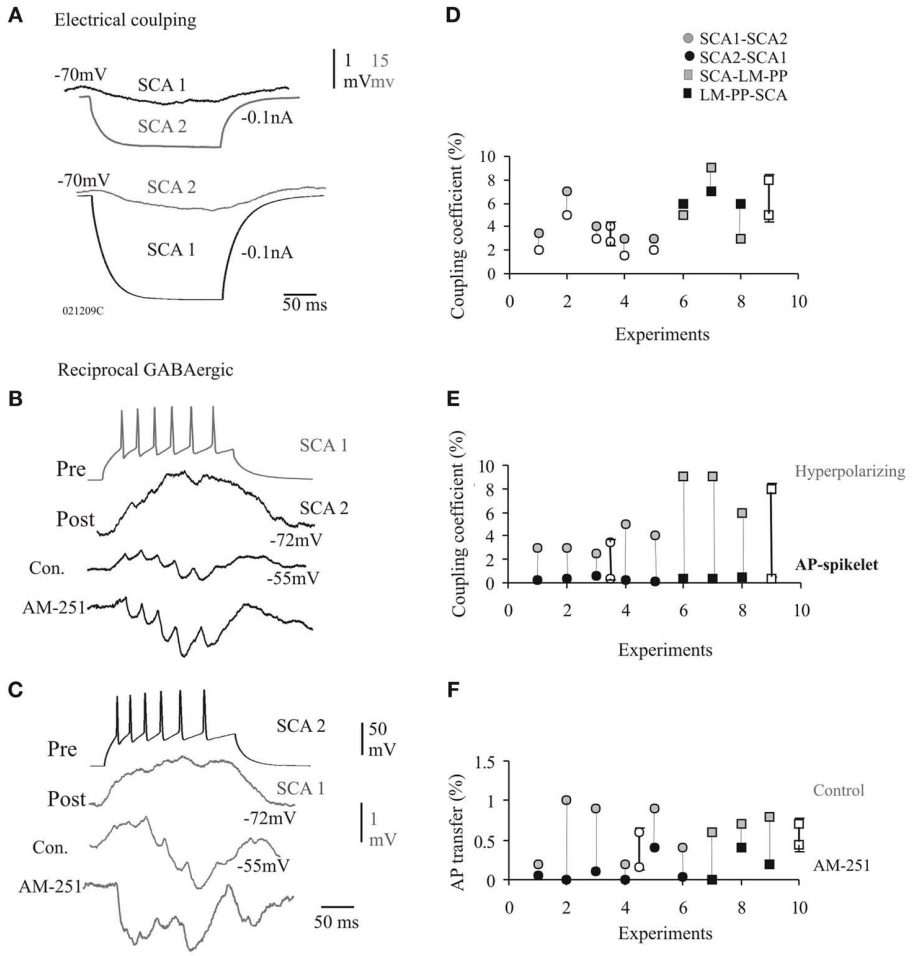

FIGURE 4 | Dual connections via electrical and chemical synapses at CCK cells. (A) The passive transfer of voltage was always reciprocal and transfer in both directions recorded at −70 mV is shown. **(B,C)** Examples of IPSPs reducing the steady-state coupling coefficients at a electrical connection between SCA and SCA cells that also received reciprocal chemical inputs. The average IPSPs elicited at −55 mV in response to a train of presynaptic action potentials displayed synaptic facilitation. These IPSPs enhanced in peak amplitude during bath application of cannabinoid type-1 (CB1) receptor antagonist, AM-251, which further reduced the passive electrical transfer. **(D)** The transfer of voltage was asymmetric at electrical synapses that were also chemically connected. **(E)** Similar to pure electrical synapses the efficiency of transmission for fast APs was lower in comparison to the hyperpolarizing phases of the APs. **(F)** The AP transfer in control and bath application of AM-251 is shown for individual pairs. The AP transfer was reduced in AM-251 (probably as a result of enhanced IPSPs). Data for individual pairs are shown in **(C,E,F)**, average values ± SE are represented by empty symbols.

DSI ENHANCES ELECTRICAL COUPLING AT ELECTRICAL SYNAPSES THAT RECEIVE CHEMICAL SYNAPTIC INPUTS

The average IPSP latency was 4.5 ± 3.6 ms during DSI and was comparable to control average latency. There was a high proportion of asynchronous release in control and during DSI and synchronicity ratios were comparable, 0.62 ± 0.53 and 0.75 ± 0.8 in control and during DSI, respectively ($p \leq 0.05$, $n = 8$, see **Figures 5A,Ai**). This maintained asynchronous release of GABA during DSI probably reflects the increased duration of the spikelets (average duration was, 46 ± 4 ms, a 200% increase) shown in **Figures 5B,Bi**).

The steady-state coupling coefficients were found to be considerably larger during the DSI protocol as DSI reduced the amplitudes of IPSPs. Average first amplitudes were reduced to, 0.12 ± 0.1 mV (95% reduction of control, $n = 5$). However, at pure electrical connections, DSI did not change the coupling coefficients, shown in **Figure 5C** (paired t-test, $p \geq 0.5$, $n = 3$). This suggests that the enhancement of electrical coupling during DSI can only be attributed to electrical synapses that are also chemically connected. **Figure 5D** illustrated the spike coupling coefficient during control and DSI. The spike coupling coefficient during DSI was, $1.06 \pm 0.25\%$ (control average value, $0.3 \pm 0.2\%$) and $0.9 \pm 0.05\%$ (average control value, $0.2 \pm 0.08\%$) for SCA–SCA and SCA–LM–PP connections, respectively. Bath application of AM-251 prevented the DSI effects as a result of larger IPSP amplitudes and on average reduced coupling coefficients to, $0.08 \pm 0.11\%$ (84% reduction of control). **Figure 5E** illustrates that larger IPSPs were related to smaller passive transfer of voltage ($r = 0.55$, $p < 0.05$, $n = 23$).

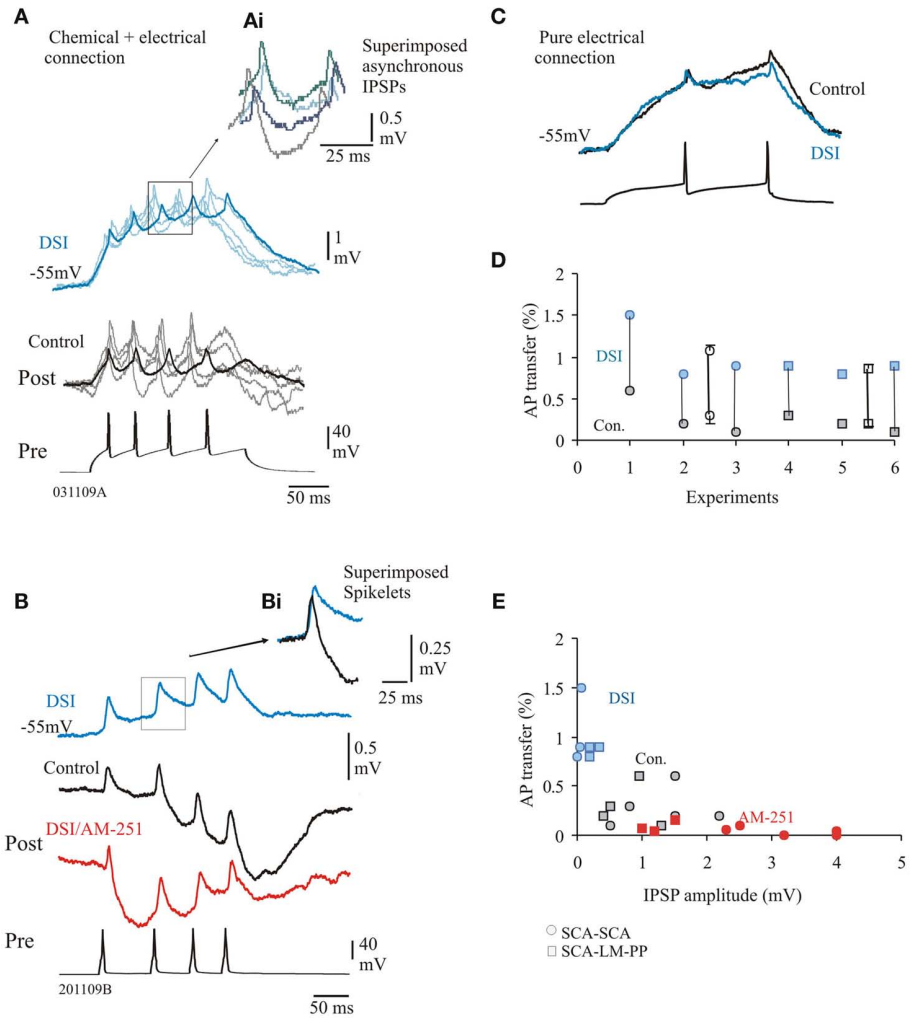

FIGURE 5 | Depolarization induced suppression of inhibition (DSI) enhances efficiency of electrical coupling. (A) SCA–SCA pair connected via electrical and chemical synapses. Faint traces represent single sweep data, bold traces are averaged responses. During DSI the efficiency of the passive transfer of voltage was stronger as DSI reduced IPSPs compared to control IPSPs. **(Ai)** superimposed single sweep IPSPs elicited during DSI show asynchronous release of GABA similar to control conditions. **(B)** Averaged biphasic IPSPs, DSI reduced averaged IPSPs (blue trace), which was prevented during bath application of AM-251. Note that AM-251 also changed facilitation to synaptic depression (see Ali, 2011, for further details). **(Bi)** Superimposed spikelets in control and DSI, enhanced transfer of amplitude and duration of the spikelets resulted during DSI. **(C)** SCA–SCA pair connected purely via electrical synapses. Averaged responses in control and during DSI are superimposed to illustrate that DSI did not enhance coupling coefficient at these synapses. **(D)** AP transfer in control and during DSI for individual pairs (average data ± SE are represented by empty symbols, *x*-axis represents individual pairs). **(E)** Plot of AP transfer and IPSP peak amplitudes, larger amplitude of the IPSPs (during AM-251, shown in red) was related to lower passive transfers.

DISCUSSION

Our results demonstrate that electrical coupling between CCK interneurons of the CA1 region occur between cells of the same morphological subclass and also connections between heterogeneous cell types. Within networks of CCK interneurons the synergy between the electrical and chemical synapses probably act as mechanisms to modulate rhythmic synchronization via activity-dependent endocannabinoid release; while DSI via CB1 receptor activation enhance and prolong electrical coupling, diminished CB1 receptor activity resulted in precisely timed enhanced inhibition leading to a decline in electrical coupling, which is perhaps a mechanism for desynchronization.

ELECTRICAL COUPLING BETWEEN MORPHOLOGICAL SUBCLASSES OF CCK INTERNEURONS

Heterogeneity in the morphology, intrinsic membrane property and expression of neuropeptides and calcium binding proteins exists between subclasses of CCK cells (Kubota and Kawaguchi, 1997; Pawelzik et al., 2002; Losonczy et al., 2004; Ali and Todorova, 2010). The asymmetry of the coupling coefficient between heterogeneous cells can not be attributed to junction rectification, but differential electrical size of the cells reflected in the differences in the input resistance. The divergent electrical coupling reported here is consistent with neocortical studies reporting electrical coupling between multipolar and bipolar calretinin cells (Caputi et al.,

2009) and between NGF cells and several other subclasses of interneurons shown to be connected via somato-dendritic coupling (Simon et al., 2005; see also Venance et al., 2000; Chu et al., 2003). Our findings support dendritic spatial computation models and the predictions that the input resistance at the dendrite of the asymmetrical model (compared to symmetrical coupling model) is directly related to the degree of asymmetric coupling that could a play important role in dendritic excitability (Kim and Jones, 2011).

Communication solely via electrical coupling between SCA cells and between SCA and other CCK interneurons here can synchronize pairs of interneurons as they were connected via putative somato-dendritic gap junctions, although the dendritic coupling between SCA and basket cells could limit the size of electrically coupled networks due to filtering properties, which is reflected by the weak spike-spike coupling displayed at these connections. Others have also reported that networks of NGF cells display weak spike-spike transmission (Galarreta and Hestrin, 1999; Gibson et al., 1999; Blatow et al., 2003; Simon et al., 2005). However, the arrangement and number of gap junctions within a single connection could influence the formation of widespread electrically activity. CCK cells that were connected between subregions, e.g., SCA–LM–PP cells probably play a role in shaping oscillatory activity across subregions of the hippocampus and the dentate gyrus since these two interneuronal groups are able to integrate excitation received from different subregions.

DSI VIA CB1 RECEPTORS ALTER ELECTRICAL COUPLING AT CCK INTERNEURONS

It has been proposed that endocannabinoids may negate inhibitory transmission at specific inputs that could disrupt synchronized oscillations in certain frequency ranges (Katona et al., 1999) and disrupt spike timing decreasing the power of neuronal oscillations (Robbe et al., 2006). This is also consistent with studies suggesting that the activation of CB1 receptors interferes with neuronal network oscillations and impairs sensory gating function in the limbic circuitry (Hajós et al., 2008). We demonstrate for the first time that DSI and CB1 receptors alter electrical coupling (that probably enhances synchronization) at connections that were coupled via both chemical and electrical synapses, but not at pure electrical synapses, suggesting two distinct populations of electrical synapses. Synapses that are both chemically and electrically coupled have been reported previously in various regions of the CNS and perhaps this dual connectivity is a general mechanism for modulating synchronization as chemical synapses were also shown to curtail electrical activity (Kosaka and Hama, 1985; Koos and Tepper, 1999; Tamas et al., 2000), our results corroborated and extended these findings. This type of modulation is perhaps an important property of CA1, CCK interneurons in controlling and setting the phasing accuracy by allowing integration of tonic inhibition modulated via CB1 receptors and electrical potentials during DSI as a high proportion of SCA–SCA cells received chemical synapses that were electrical coupled.

Previously it has been demonstrated that DSI is mediated via retrograde release of endocannabinoids from the postsynaptic cell (Ohno-Shosaku et al., 2001; Wilson and Nicoll, 2001; Ali, 2007). In the absence of CB1 receptor activity, tonic suppression of inhibition resulting in periods of enhanced inhibition negated the transfer of electrical potentials, suggesting that CB1 receptors play an important role in modulating electrical transfer. Irregular-spiking interneurons that expressed CB1 receptors and sensitive to CB1 receptor pharmacology have been reported to be electrically coupled in the neocortex (Galarreta et al., 2004), although these electrically coupled cells did not display asymmetric coupling coefficients and were solely coupled electrically.

It is interesting to note that connections between CCK and postsynaptic pyramids and interneurons show marked asynchronous release (Hefft and Jonas, 2005; Galarreta et al., 2008; Karson et al., 2009; Ali and Todorova, 2010; Daw et al., 2010). Asynchronous release, where a presynaptic action potential loosely coupled to vesicle release or postsynaptic activation, may be consequential to the nature of synaptic transmission; a temporally dispersed GABA concentration transient may confer a tonic, rather than phasic, response. This is in contrast to fast spiking parvalbumin positive interneurons which show tightly coupled release (synchronous) to the presynaptic action potential; this reflects the importance of CCK interneurons in providing a temporal framework for excitability in the postsynaptic cell (Hefft and Jonas, 2005; Glickfeld and Scanziani, 2006). Other differences between CCK interneurons in CA1 compared to the inhibitory network of fast spiking, parvalbumin cells include their slower time courses of IPSPs and short-term dynamics. Communication among CCK cells displays synaptic facilitation (Ali, 2011; see also Losonczy et al., 2004; Hefft and Jonas, 2005), in contrast to depression observed at CCK and parvalbumin cells connected to postsynaptic pyramidal cells and between parvalbumin cells (Tamas et al., 2000; Galarreta et al., 2008). These properties unique to the inhibitory network of CCK interneurons, i.e., synaptic facilitation and asynchronous release between CCK cells in CA1 have been shown to be governed by CB1 receptors (Ali and Todorova, 2010). Together these studies illustrate that fast spiking and CCK inhibitory network are different in their synaptic properties which translate to their functional roles in the network. Electrical coupling between fast spiking parvalbumin cells aids fast rhythmic synchronous entrainment of action potential firing, aiding the stability of oscillatory network activity/temporal pattern formation (Tamas et al., 2000), whereas CCK cells which are connected via electrical and chemical synapses may allow desynchronization of this fast rhythmic activity as the chemical synaptic activity is governed by the powerful modulator endocannabinoids.

In conclusion we report two differentially connected CCK interneuronal networks; communication solely via electrical coupling between heterogeneous cell types and electrically coupled cells which also receive chemical inputs, thereby providing two distinct functional inputs. The electrical coupling between CCK cells of different subtypes may play an important role in shaping network oscillations as they are able to coordinate and integrate excitation from different hippocampal sub regions. CCK cells involved in fine temporal encoding of the postsynaptic cells and rhythm generation are influenced by many factors including; asynchronous release, strength of inhibition (modulated via DSI/CB1 receptors) and electrical coupling. These factors probably influence synchronization/desynchronization in an activity-dependent release of endocannabinoid release in CA1.

ACKNOWLEDGMENTS

This project was funded by the Medical Research Council (UK), New Investigators Award, awarded to Dr AB Ali. Mr Jonathan Iball was involved in the anatomical aspect of this project. We would like to thank Prof. Alex Thomson for financially supporting Mr Jonathan Iball. CCK antibody used in this study was a gift from Dr Gordon Ohning, UCLA.

REFERENCES

Ali, A. B. (2007). Presynaptic inhibition of GABAA receptor-mediated unitary IPSPs by cannabinoid receptors at synapses between CCK-positive interneurons in rat hippocampus. *J. Neurophysiol.* 98, 861–869.

Ali, A. B. (2011). CB1 modulation of temporally distinct synaptic facilitation among local circuit interneurons mediated by N-type calcium channels in CA1. *J. Neurophysiol.* 105, 1051–1062.

Ali, A. B., Bannister, A. P., and Thomson, A. M. (1999). IPSPs elicited in CA1 pyramidal cells by putative basket cells in slices of adult rat hippocampus. *Eur. J. Neurosci.* 11, 1741–1753.

Ali, A. B., and Todorova, M. (2010). Asynchronous release of GABA via tonic cannabinoid receptor activation at identified interneuron synapses in rat CA1. *Eur. J. Neurosci.* 31, 1196–1207.

Best, A. R., and Regehr, W. G. (2009), Inhibitory regulation of electrically coupled neurons in the inferior olive is mediated by asynchronous release of GABA. *Neuron* 62, 555–565.

Blatow, M., Rozov, A., Katona, I., Hormuzdi, S. G., Meyer, A. H., Whittington, M. A., Caputi, A., and Monyer, H. (2003). A novel network of multipolar bursting interneurons generates theta frequency oscillations in neocortex. *Neuron* 38, 805–817.

Bodor, A. L., Katona, I., Nyiri, G., Mackie, K., Ledent, C., Hajos, N., and Freund, T. F. (2005). Endocannabinoid signaling in rat somatosensory cortex: laminar differences and involvement of specific interneuron types. *J. Neurosci.* 25, 6845–6856.

Caputi, A., Rozov, A., Blatow, M., and Monyer, H. (2009). Two calretinin-positive GABAergic cell types in layer 2/3 of the mouse neocortex provide different forms of inhibition. *Cereb. Cortex* 19, 1345–1359.

Chu, Z., Galarreta, M., and Hestrin, S. (2003). Synaptic interactions of late-spiking neocortical neurons in layer 1. *J. Neurosci.* 23, 96–102.

Cobb, S. R., Buhl, E. H., Halasy, K., Paulsen, O., and Somogyi, P. (1995). Synchronization of neuronal activity in hippocampus by individual GABAergic interneurons. *Nature* 378, 75–78.

Daw, M. I., Pelkey, K. A., Chittajallu, R., and McBain, C. J. (2010). Presynaptic kainate receptor activation preserves asynchronous GABA release despite the reduction in synchronous release from hippocampal cholecystokinin interneurons. *J. Neurosci.* 30, 11202–11209.

Freund, T. F., and Buzsaki, G. (1996). Interneurons of the hippocampus. *Hippocampus* 6, 347–470.

Galarreta, M., Erdelyi, F., Szabo, G., and Hestrin, S. (2004). Electrical coupling among irregular-spiking GABAergic interneurons expressing cannabinoid receptors. *J. Neurosci.* 24, 9770–9778.

Galarreta, M., Erdelyi, F., Szabo, G., and Hestrin, S. (2008). Cannabinoid sensitivity and synaptic properties of 2 GABAergic networks in the neocortex. *Cereb. Cortex* 18, 2296–2305.

Galarreta, M., and Hestrin, S. (1999). A network of fast-spiking cells in the neocortex connected by electrical synapses. *Nature* 402, 72–75.

Gibson, J. R., Beierlein, M., and Connors, B. W. (1999). Two networks of electrically coupled inhibitory neurons in neocortex. *Nature* 402, 75–79.

Glickfeld, L. L., and Scanziani, M. (2006). Distinct timing in the activity of cannabinoid-sensitive and cannabinoid-insensitive basket cells. *Nat. Neurosci.* 9, 807–815.

Hajós, M., Hoffmann, W. E., and Kocsis, B. (2008). Activation of cannabinoid-1 receptors disrupts sensory gating and neuronal oscillation: relevance to schizophrenia. *Biol. Psychiatry* 63, 1075–1083.

Hajós, N., Katona, I., Naiem, S. S., Mackie, K., Ledent, C., Mody, I., and Freund, T. F. (2000). Cannabinoids inhibit hippocampal GABAergic transmission and network oscillations. *Eur. J. Neurosci.* 12, 3239–3249.

Hefft, S., and Jonas, P. (2005). Asynchronous GABA release generates long-lasting inhibition at a hippocampal interneuron-principal neuron synapse. *Nat. Neurosci.* 8, 1319–1328.

Hjorth, J., Blackwell, K. T., and Kotaleski, J. H. (2009). Gap junctions between striatal fast-spiking interneurons regulate spiking activity and synchronization as a function of cortical activity. *J. Neurosci.* 29, 5276–5286.

Hormuzdi, S. G., Pais, I., LeBeau, F. E., Towers, S. K., Rozov, A., Buhl, E. H., Whittington, M. A., and Monyer, H. (2001). Impaired electrical signaling disrupts gamma frequency oscillations in connexin 36-deficient mice. *Neuron* 31, 487–495.

Karson, M. A., Tang, A. H., Milner, T. A., and Alger, B. E. (2009). Synaptic cross talk between perisomatic-targeting interneuron classes expressing cholecystokinin and parvalbumin in hippocampus. *J. Neurosci.* 29, 4140–4154.

Katona, I., Sperlagh, B., Sik, A., Kafalvi, A., Vizi, E. S., Mackie, K., and Freund, T. F. (1999). Presynaptically located CB1 cannabinoid receptors regulate GABA release from axon terminals of specific hippocampal interneurons. *J. Neurosci.* 19, 4544–4558.

Kim, H., and Jones, K. E. (2011). Asymmetric electrotonic coupling between the soma and dendrites alters the bistable firing behaviour of reduced models. *J. Comput. Neurosci.* 30, 659–674.

Koos, T., and Tepper, J. M. (1999). Inhibitory control of neostriatal projection neurons by GABAergic interneurons. *Nat. Neurosci.* 2, 467–472.

Kosaka, T., and Hama, K. (1985). Gap junctions between non-pyramidal cell dendrites in the rat hippocampus (CA1 and CA3 regions): a combined Golgi-electron microscopy study. *J. Comp. Neurol.* 231, 150–161.

Kubota, Y., and Kawaguchi, Y. (1997). Two distinct subgroups of cholecystokinin-immunoreactive cortical interneurons. *Brain Res.* 752, 175–183.

Llano, I., Leresche, N., and Marty, A. (1991). Calcium entry increases the sensitivity of cerebellar Purkinje cells to applied GABA and decreases inhibitory synaptic currents. *Neuron* 6, 565–574.

Losonczy, A., Biro, A. A., and Nusser, Z. (2004). Persistently active cannabinoid receptors mute a subpopulation of hippocampal interneurons. *Proc. Natl. Acad. Sci. U.S.A.* 101, 1362–1367.

Mancilla, J. G., Lewis, T. J., Pinto, D. J., Rinzel, J., and Connors, B. W. (2007). Synchronization of electrically coupled pairs of inhibitory interneurons in neocortex. *J. Neurosci.* 27, 2058–2073.

Marsicano, G., and Lutz, B. (1999). Expression of the cannabinoid receptor CB1 in distinct neuronal subpopulations in the adult mouse forebrain. *Eur. J. Neurosci.* 11, 4213–4225.

Ohno-Shosaku, T., Maejima, T., and Kano, M. (2001). Endogenous cannabinoids mediate retrograde signals from depolarized postsynaptic neurons to presynaptic terminals. *Neuron* 29, 729–738.

Pappas, G. D., and Bennett, M. V. (1966). Specialized junctions involved in electrical transmission between neurons. *Ann. N. Y. Acad. Sci.* 137, 495–508.

Pawelzik, H., Hughes, D. I., and Thomson, A. M. (2002). Physiological and morphological diversity of immunocytochemically defined parvalbumin- and cholecystokinin-positive interneurones in CA1 of the adult rat hippocampus. *J. Comp. Neurol.* 443, 346–367.

Robbe, D., Montgomery, S. M., Thome, A., Rueda-Orozco, P. E., McNaughton, B. L., and Buzsaki, G. (2006). Cannabinoids reveal importance of spike timing coordination in hippocampal function. *Nat. Neurosci.* 9, 1526–1533.

Simon, A., Olah, S., Molnar, G., Szabadics, J., and Tamas, G. (2005). Gap-junctional coupling between neurogliaform cells and various interneuron types in the neocortex. *J. Neurosci.* 25, 6278–6285.

Sloper, J. J. (1972). Gap junctions between dendrites in the primate neocortex. *Brain Res.* 44, 641–646.

Somogyi, P., and Klausberger, T. (2005). Defined types of cortical interneurone structure space and spike timing in the hippocampus. *J. Physiol. (Lond.)* 562, 9–26.

Tamas, G., Buhl, E. H., Lorincz, A., and Somogyi, P. (2000). Proximally targeted GABAergic synapses and gap junctions synchronize cortical interneurons. *Nat. Neurosci.* 3, 366–371.

Venance, L., Rozov, A., Blatow, M., Burnashev, N., Feldmeyer, D., and Monyer, H. (2000). Connexin expression in electrically coupled postnatal rat brain neurons. *Proc. Natl. Acad. Sci. U.S.A.* 97, 10260–10265.

Wilson, R. I., and Nicoll, R. A. (2001). Endogenous cannabinoids mediate retrograde signalling at hippocampal synapses. *Nature* 410, 588–592.

Conflict of Interest Statement: The authors declare that the research was conducted in the absence of any commercial or financial relationships that could be construed as a potential conflict of interest.

Received: 15 September 2011; accepted: 07 November 2011; published online: 22 November 2011.

Citation: Iball J and Ali AB (2011) Endocannabinoid release modulates electrical coupling between CCK cells connected via chemical and electrical synapses in CA1. Front. Neural Circuits ***5****:17. doi: 10.3389/fncir.2011.00017*